

Anomalous Underscreening in the Restricted Primitive Model

Andreas Härtel¹, Moritz Bültmann¹, and Fabian Coupette¹

Institute of Physics, University of Freiburg, Hermann-Herder-Straße 3, 79104 Freiburg, Germany

(Received 7 September 2022; revised 19 December 2022; accepted 8 February 2023; published 9 March 2023)

Underscreening is a collective term for charge correlations in electrolytes decaying slower than the Debye length. Anomalous underscreening refers to phenomenology that cannot be attributed alone to steric interactions. Experiments with concentrated electrolytes and ionic fluids report anomalous underscreening, which so far has not been observed in simulation. We present Molecular Dynamics simulation results exhibiting anomalous underscreening that can be connected to cluster formation. A theory that accounts for ion pairing confirms the trend. Our results challenge the classic understanding of dense electrolytes impacting the design of technologies for energy storage and conversion.

DOI: [10.1103/PhysRevLett.130.108202](https://doi.org/10.1103/PhysRevLett.130.108202)

In recent years, unexpectedly long decay lengths of electrostatic forces have been observed in concentrated electrolytes [1–8] subsumed under the term “underscreening.” A lot of effort has been committed to explaining underscreening [9–25]. We distinguish regular underscreening that can be attributed to steric interactions from anomalous underscreening characterized by much longer decay lengths compared to its regular counterpart. Numerous studies have concluded that one of the most fundamental models for electrolytes and ionic liquids, the restricted primitive model (RPM), does not exhibit anomalous underscreening. As even some experimental studies could not find these large decay lengths [25,26], the phenomenon itself has been questioned. In this Letter, we demonstrate that there is anomalous underscreening in the RPM using Molecular Dynamics simulations. However, our findings do not support a unique scaling of decay lengths as reported in [10,11]. We can explain our directly measured results with cluster formation, which effectively reduces the concentration of mobile charge carriers. Finally, we propose a minimal theory of ion pairing that captures the phenomenology and even provides sensible agreement with the experiment.

In an ionic fluid, the Coulomb interaction between two charged particles is exponentially screened due to the presence of mobile charge carriers. The screening length is the inverse decay rate of this exponential, which reflects the ability of an electrolyte to screen surface charges on electrodes. Accordingly, it is closely related to the formation of electric double layers, which play a fundamental role in, among others, modern charge storing, energy conversion, and desalination technologies [27–30], chemical and colloidal interactions [31–33], and DNA [34,35], as well as nervous conduction [36,37]. The strength of electrostatic interactions is encoded in the Bjerrum length $\lambda_B = e^2/(4\pi\epsilon_0\epsilon k_B T)$, with elementary charge e , vacuum

permittivity ϵ_0 , the relative dielectric permittivity of the solvent ϵ , and Boltzmann’s constant k_B .

The expected decay length for dilute systems of charged particles is given by the Debye screening length $\lambda_D = 1/\sqrt{8\pi\rho_s\lambda_B}$ [38] that decreases with increasing number density ρ_s of mobile charges and with the Bjerrum length. By convention, ρ_s is the individual density of positive and negative charges, respectively, and often given as salt concentration c . Underscreening refers to a less effective screening, i.e., decay lengths exceeding the Debye length that have been observed by surface force apparatus (SFA) experiments for high salt concentrations or large Bjerrum lengths [1].

However, the experiments report that the charge correlation is the sum of two qualitatively different decays: a potentially oscillatory structural decay at small distances and a much slower long-ranged strictly nonoscillatory decay at greater separations [39]. The structural decay is well understood theoretically within the RPM of charged hard spheres and originates from the interplay between electrostatic and steric interactions of the particles (see Ref. [24] and references therein).

From simulations of the monovalent RPM, we can extract the charge correlation as $h_{cc} = g_{++} - g_{+-}$, where $g_{\mu\nu}$ denotes the species resolved pair-distribution function. In theory, these pair-distribution functions can be obtained from the Ornstein-Zernike equation that defines their analytic structure. The charge correlation can be expressed as an infinite sum over terms of the form

$$H_i(r) = A_i \exp(-r/\lambda_i) \cos(\omega_i r + \tau_i)/r^{b_i}, \quad (1)$$

with decay or screening length λ_i , amplitude A_i , ω_i and τ_i describing potential oscillations, and $b_i \in \{1, 2\}$. Each term originates from a complex singularity of an auxiliary function, $b_i = 1$ applies for simple poles [40–43], and

$b_i = 2$ for branch points [44,45]. Further details are given in the Supplemental Material [46]. At long separations r the contribution with the longest decay length λ_i dominates. With increasing salt concentration, the dominant exponential decay switches from monotonic to oscillatory (Kirkwood crossover) [61,62] as well as from charge to density dominated [15], depending on the ionic diameter.

It needs to be emphasized that the structural decay observed in the experiments already shows underscreening. This *regular* underscreening has been observed in simulations and the underlying mechanism is theoretically well understood.

In contrast to that, the long-ranged decay was found exclusively in a few experimental studies. Recent works concluded that the RPM that accurately explains the structural decay is incapable of predicting the long-ranged decay [18,21,24,25], which we refer to as *anomalous* underscreening. Thus, either the RPM is missing a crucial ingredient or the long-ranged decay is an artifact of the experiment. Within this Letter we show that there is a third option.

Underscreening is often categorized by power laws of the form $\lambda/\lambda_D \sim (\sigma/\lambda_D)^p$, with ion diameter σ , even though the available data do not cover a single decade. Regular underscreening corresponds to $p \approx 3/2$, while $p \approx 3$ is anomalous. The SFA results suggest that λ/λ_D depends uniquely on the dimensionless quantity $\kappa = \sigma/\lambda_D$, because data for many different electrolytes and ionic liquids all collapse onto one unique curve [10]. This conclusion, however, is misleading. Figure 1 illustrates the phase

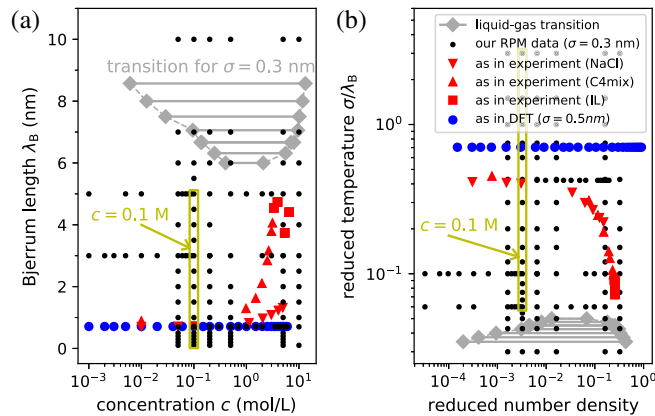


FIG. 1. Phase diagram of the RPM for (a) the concentration c and Bjerrum length λ_B and (b) for reduced temperature $T^* = \sigma/\lambda_B$ and total number density $\rho^* = 2\rho_s\sigma^3$. Each symbol marks a parameter set for which we have run MD simulations. The data points for $c = 0.1$ mol/L and $\lambda_B = 0.1, \dots, 5.0$ nm are highlighted by an orange rectangle. Special symbols show the sets used in a previous theoretical study (DFT) [24] and in experiments [5] with NaCl in water (NaCl), [C4C1Pyr][NTf2] in propylene carbonate (C4mix), and an ionic liquid (IL) (further details in the Supplemental Material [46]). Horizontal lines mark the region of liquid-gas phase coexistence [63]; see Ref. [64] for further phases.

diagram of the RPM in (a) dimensional and (b) reduced dimensionless units. Every small circle marks a parameter set (c, λ_B) for which we performed Molecular Dynamics (MD) simulations. The triangles and squares correspond to parameters as used in the SFA experiments for different electrolytes and ionic liquids. Curiously, in reduced units all experimentally probed parameter sets collapse onto one curve in the phase diagram. Thus, it is not surprising that the resulting decay lengths do the same.

Simulation and theoretical studies typically explore underscreening by solely varying the concentration exemplified by the large circles in Fig. 1. Conversely, the experimental parameters that exhibit anomalous underscreening at large concentrations predominantly vary in the Bjerrum length. Thus, previous studies only explore limited parts of parameter space. To address this issue, we present MD simulations for a wide range of parameters comprehensively screening the phase diagram as illustrated in Fig. 1. In particular, this allows us to extract the decay length as a function of the Bjerrum length for several fixed concentrations. For each set of parameters (c, λ_B) we run MD simulations of the RPM with $\sigma = 0.3$ nm [further details in the Supplemental Material [46]; the typical size of the cubic simulation box is $(60 \text{ nm})^3$. Once equilibrated, we sample the radial pair-distribution functions $g_{\mu\nu}(r)$ and compute the charge correlation h_{cc} . To extract the principal decay lengths, we fit h_{cc} to a superposition of decays H_i [Eq. (1)] accounting for up to three poles and a potential branch point—Fig. 2 exemplifies the procedure.

The representation $\log(r|h_{cc}|)$ is chosen in accordance with the known form of the decay in Eq. (1) so that the decay length corresponds to the slope of a linear fit. In Fig. 2, we find the two previously discussed decay regimes: the structural decay (up to $r \approx 1.5$ nm) and long-ranged

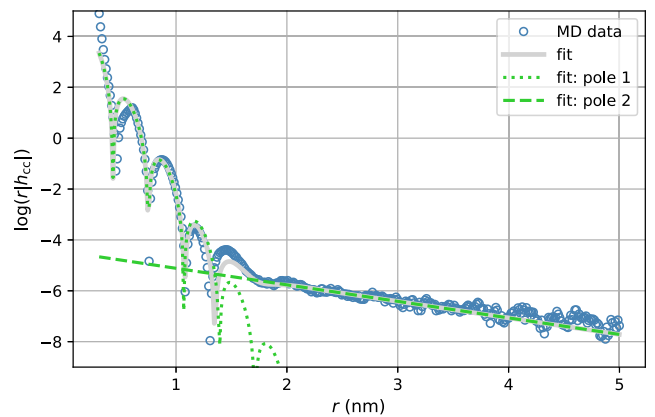


FIG. 2. Charge-correlation function $h_{cc}(r)$ in a representation that shows the decay length as the slope of the graph. This function was sampled by a MD simulation with $c = 0.1$ mol/L, $\lambda_B = 5$ nm, and $\sigma = 0.3$ nm. The pole fits have the analytical form of Eq. (1), respectively (see Supplemental Material [46] for further details on the fits).

decay ($r \gtrsim 1.5$ nm). Consistent with the SFA measurements, the long-ranged decay (pole 2) is always found to be monotonic, while the structural decay (pole 1) can also show oscillations depending on the parameters. At very large separations, the decay with the largest decay length dominates. However, in the Supplemental Material [46] we demonstrate that the amplitude A_i of this dominant contribution may be small such that the signal is buried in statistical noise of the simulations. This complicates the extraction of decay lengths, particularly for large concentrations. Details on the simulations and fitting procedure including the fitted parameters for all charge correlations can be found in [46].

In Fig. 3, we present the measured decay lengths that we obtained from our MD simulations at fixed concentration $c = 0.05/0.1/0.2/0.5$ mol/L, respectively (results for all parameter pairs presented in Fig. 1 are shown in the Supplemental Material [46]). Our broad exploration of the phase diagram reveals that there is no unique relationship in reduced parameters. The decay length generally depends on salt concentration and Bjerrum length, independently. If we increase the Bjerrum length at fixed concentration, we find λ_2 being the Debye length at small σ/λ_D but approximately following a power law $\lambda_2 \sim (\sigma/\lambda_D)^3$ at larger σ/λ_D , as observed in the experiments for dense electrolytes. Each λ_2 is accompanied by a much shorter decay length λ_1 that describes structural screening.

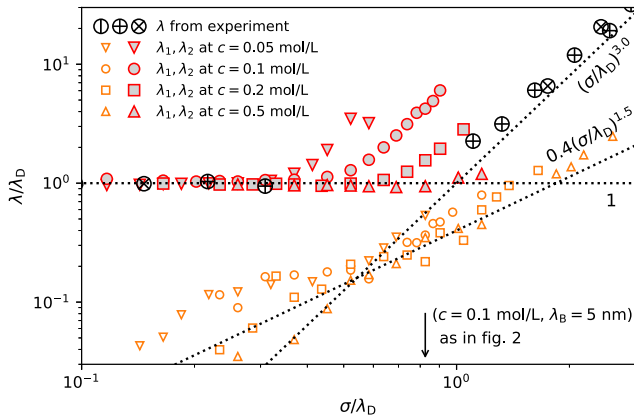


FIG. 3. Decay lengths λ_1 and λ_2 obtained by fitting $\sum_{i=1}^n H_i(r)$, $n \in \{1, 2, 3\}$ to bulk charge-correlation functions sampled from our MD simulations of the RPM as exemplarily shown in Fig. 2. λ_1 represents decay lengths of the structural decay and λ_2 represents decay lengths of the long-ranged monotonic decay (compare poles 1 and 2 in Fig. 2). Note that in some cases we used a third pole for the fit [46]. We show the decay length λ in relation to the Debye length λ_D against σ/λ_D (depending on λ_B and c), as common in the literature on underscreening [11]. For each given concentration, we varied only the Bjerrum length. Large black circles represent data from experiments on an ionic liquid (\circ), NaCl in water ($+$), and [C4C1Pyr][NTf2] in propylene carbonate (\times) [5]. Dotted lines depict power laws as noted.

All structural decay lengths λ_1 approximately follow a power law $\lambda_1 \sim (\sigma/\lambda_D)^{1.5}$, as demonstrated in Fig. 3.

The curves of λ_2 at fixed concentration that show anomalous underscreening shift to the right in Fig. 3 with increasing concentration. At the same time, the amplitude of the decay H_2 from Eq. (1) decreases with increasing concentration. At high concentrations, the decay $H_2(r)$ drops below the numerical resolution of our MD simulation (see Ref. [46] for further details). For reference, we also show experimental results for different ionic liquids and electrolytes in Fig. 3. Varying the concentration, we only find regular underscreening in the dense regime (data not shown). The extracted decay lengths approximately follow the power law $0.4(\sigma/\lambda_D)^{1.5}$ (Fig. 3), which is consistent with the literature [24].

In conclusion, there is anomalous underscreening in the RPM but it cannot be observed in simulations for parameters suggested by the experiment.

However, if there is anomalous underscreening in the RPM, theoretical approaches should find it as well. Recently, Cats *et al.* presented a comprehensive comparison between available theoretical results and concluded that classical density functional theory (DFT) is a good approach to describe screening in electrolytes and ionic liquids [24]. Classical DFT accurately predicts the structural decay, i.e., regular underscreening [15,24,25,65]. However, DFT calculations for a fixed concentration $c = 0.1$ mol/L and varying Bjerrum length do not show anomalous underscreening [46], in contrast to our MD simulations (Fig. 3). The predictions of classical DFT reflect the accuracy of the employed excess free energy functional. It stands to reason that the theory does simply not account for the mechanism that causes anomalous underscreening.

Candidates for missing ingredients in the theoretical description are the subject of ongoing discussions. Theoretical models are frequently criticized for their implicit treatment of solvents that can significantly alter the effective steric and electrostatic interactions between ions. However, anomalous underscreening has been reported experimentally for a variety of very different solvents and even for ionic liquids. Moreover, simulations that explicitly accounted for atomistic solvent did not observe anomalous underscreening [18]. A promising contender is a reduction of the concentration of effective charge carriers, for instance, by the formation of Bjerrum pairs or by defects in dense electrolytes taking over the role of mobile charges [1,7,23,66–74]. To estimate the effective concentration of free charge carriers, we analyze system configurations generated by our MD simulations for cluster formation.

To this end, we assign a connectivity shell of diameter $d > \sigma$ to all particles in our simulation and consider two particles connected if their respective connectivity shells overlap. The clusters detected in this way either comprise

the same number of positive and negative charges, such that their collective contribution to screening is supposedly negligible, or have a finite net charge. Based on our cluster results, we safely assume that the absolute net charge of a cluster is either one elementary charge or zero [46]. In consequence, we define free ions by neglecting all clusters that contain an even number of particles and by replacing each cluster that contains an odd number of particles by one free (nonclustered) ion. With increasing Bjerrum length, the fraction of free ions decreases.

We now assume that only free particles contribute to screening and split the number density ρ_s of all ions into free and bound parts, $\rho_s = \rho_f + \rho_b$. Assuming only the free ions cause Debye screening, the expected decay length is simply the Debye length for the reduced density ρ_f , $\lambda^{\text{MD},f} = 1/\sqrt{8\pi\lambda_B\rho_f}$. In Fig. 4(a), the decay lengths resulting from this cluster analysis on the same simulation data that led to the results of Fig. 3 are displayed for different connectivity shell diameters $d = 1.5\sigma, 2\sigma, 3\sigma$ alongside the directly measured decay length λ_2 from Fig. 3. Our cluster analysis predicts anomalous underscreening very similar to the direct extraction of decay lengths from simulation in Fig. 3. It even predicts anomalous underscreening for data points (c, λ_B) where we could not use the direct fitting method due to insufficient numerical resolution. The cluster analysis also shows anomalous underscreening in Fig. 4(b) for the same parameter pairs (c, λ_B) as used in the experiments of [5]. With an adequate choice of connectivity diameter, this prediction even matches the experimentally measured decay lengths. However, while the predicted decay length is rather insensitive to the choice of connectivity diameter d at low concentrations, which is a necessary condition for a meaningful trend as d itself has no physical footing, at higher concentrations the choice of the connectivity diameter matters, rendering the method inapplicable. A better definition of free and bound ions might be facilitated by machine-learned local structures [71,74]. Nevertheless, our cluster analysis supports the hypothesis that anomalous underscreening is also present at high concentrations in our MD simulations, but its signal is too small to be distinguished from noise [46].

To supplement our explanation of anomalous underscreening, we present a minimal theory that allows ion pairing, similar to previous approaches [66,69]. We acknowledge that the general mechanism is presumably “not a question of pair formation, but a more general transient association of ions involving several ions of opposite charge” [13]. Our approach is based on the grand canonical description of an electrolyte of positive and negative point charges in a volume V , where particles either are free or bound in neutral pairs, $\beta\Omega^{\text{pair}}/V = 2\rho_f[\log(\rho_f\Lambda_f^3) - 1] + \rho_p[\log(\rho_p\Lambda_p^3) - 1] + F^{\text{es}} - \beta\mu_f\rho_f - \beta\mu_p\rho_p$. We eliminate the thermal wavelengths by

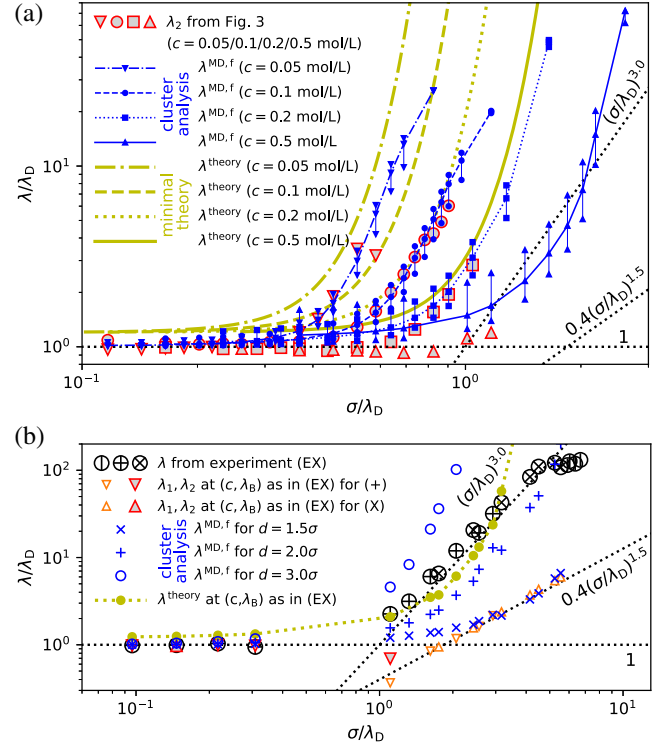


FIG. 4. Decay lengths represented as in Fig. 3. (a) Symbols without lines show decay lengths of anomalous underscreening (λ_2 in Fig. 3) as obtained by fitting the charge-correlation functions from our MD simulations of the RPM. Triplets of vertically arranged blue symbols show decay lengths $\lambda^{\text{MD},f}$ induced by free ions for different connectivity lengths $d = 1.5\sigma, d = 2\sigma, d = 3\sigma$ (from top to bottom) in the cluster search algorithm. Yellow lines show the prediction λ^{theory} of our minimal theory. (b) Directly measured λ_1 and λ_2 obtained by fitting the charge-correlation functions sampled from our MD simulations for parameter pairs (c, λ_B) as used in the experiments (EX) of [5]. The experimental data are described in Fig. 3 and also listed in the Supplemental Material [46]. Blue symbols show the resulting $\lambda^{\text{MD},f}$ from our cluster analysis for the same parameters. Yellow symbols (line added for clarity) show the corresponding λ^{theory} from our minimal theory.

identifying $\Lambda_s = \Lambda_f = \Lambda_p\sqrt{2}$ and comparing with a system of solely pointlike ions. Using $3/2k_B T$ and the electrostatic bulk energy density $F^{\text{es}} = -\lambda_D^{-3}/(12\pi)$ [38] for the internal energy per volume in units of $k_B T$, we obtain our final result

$$\beta\frac{\Omega^{\text{pair}}}{V} = 2\rho_f[\log(\rho_f/\rho_s) - 1] + \rho_p[\log(\rho_p/(\sqrt{2}^3\rho_s) - 1] - \left(1 - \frac{3\rho_f}{2\rho_s}\right)\frac{\sqrt{8\pi\lambda_B\rho_s^3}}{12\pi} + \frac{3}{2}\rho_p, \quad (2)$$

as derived in more detail in the Supplemental Material [46]. Setting $\rho_f = \alpha\rho_s$ and $\rho_p = (1 - \alpha)\rho_s$ in Eq. (2), we obtain

$\Omega^{\text{pair}}(\alpha)$ with $\alpha \in [0, 1]$ that can be minimized with respect to the fraction α of free ions while ρ_s is kept fixed.

As previously, in the cluster analysis of our simulation results, we assume that only free ions contribute to the screening of charges. Accordingly, we use the predicted density ρ_f^{theory} of free ions to obtain the decay length $\lambda^{\text{theory}} = 1/\sqrt{8\pi\lambda_B\rho_f^{\text{theory}}}$ as a function of the total ion concentration ρ_s and the Bjerrum length λ_B . In Fig. 4, we sketch the predictions of this theory of ion pairing in comparison to our results from MD simulations and experimental data. Clearly, our minimal theory predicts an even stronger increase of the decay length than is found in simulations or experiments. While this increase starts at lower σ/λ_D than expected [see Fig. 4(a)], the theory confirms the shift to larger σ/λ_D with increasing ion concentration. In Fig. 4(b), the theory reproduces the strong increase of the experimentally reported decay lengths and its position in the plot remarkably well.

In summary, we show that anomalous underscreening, which previously has only been reported experimentally, can also be found in the RPM using MD simulations. Our results demonstrate that the decay length is, in general, not a unique function of the parameter σ/λ_D as suggested by experiments [10], but the experiments probe only a unique line in the phase diagram of the RPM. On top of that, we illustrate that cluster formation induces a strong increase of the screening length, which provides an explanation for anomalous underscreening. We support this explanation, on the one hand, by analyzing clusters in our MD simulations and, on the other hand, by applying a minimal cluster theory of ion pairing which allows ions to form neutral pairs.

Finally, the question remains why some experiments could find anomalous underscreening and others could not. As a possible answer, it has been proposed that the atomic force microscope has by construction a much lower sensitivity than the SFA [1,75]. Accordingly, the signal of anomalous underscreening might be too small for some of the experiments, similar to the sensitivity of our MD simulations [46].

We thank Patrick Warren, Fabian Glatzel, and Anja Kuhnhold for fruitful discussions. A. H. and M. B. acknowledge funding from the German Research Foundation (DFG) through Project No. 406121234. F. C. acknowledges funding from the German Research Foundation (DFG) through Project No. 457534544. We acknowledge support by the state of Baden-Württemberg through bwHPC and the German Research Foundation (DFG) through Grant No. INST 39/963-1 FUGG (bwForCluster NEMO).

* andreas.haertel@physik.uni-freiburg.de

[1] M. A. Gebbie, M. Valtiner, X. Banquy, E. T. Fox, W. A. Henderson, and J. N. Israelachvili, *Proc. Natl. Acad. Sci. U.S.A.* **110**, 9674 (2013).

- [2] M. A. Gebbie, H. A. Dobbs, and M. Valtiner, and J. N. Israelachvili, *Proc. Natl. Acad. Sci. U.S.A.* **112**, 7432 (2015).
- [3] H.-W. Cheng, P. Stock, B. Moeremans, T. Baimpos, X. Banquy, F. U. Renner, and M. Valtiner, *Adv. Mater. Interfaces* **2**, 1500159 (2015).
- [4] R. M. Espinosa-Marzal, A. Arcifa, A. Rossi, and N. D. Spencer, *J. Phys. Chem. Lett.* **5**, 179 (2014).
- [5] A. M. Smith, A. A. Lee, and S. P. Perkin, *J. Phys. Chem. Lett.* **7**, 2157 (2016).
- [6] N. Hjalmarrsson, R. Atkin, and M. W. Rutland, *Chem. Commun.* **53**, 647 (2017).
- [7] A. M. Smith, P. Maroni, G. Trefalt, and M. Borkovec, *J. Phys. Chem. B* **123**, 1733 (2019).
- [8] P. Gaddam and W. Ducker, *Langmuir* **35**, 5719 (2019).
- [9] M. A. Gebbie, A. M. Smith, H. A. Dobbs, A. A. Lee, G. G. Warr, X. Banquy, M. Valtiner, M. W. Rutland, J. N. Israelachvili, S. Perkin, and R. Atkin, *Chem. Commun.* **53**, 1214 (2017).
- [10] A. A. Lee, C. S. Perez-Martinez, A. M. Smith, and S. Perkin, *Phys. Rev. Lett.* **119**, 026002 (2017).
- [11] A. A. Lee, C. S. Perez-Martinez, A. M. Smith, and S. Perkin, *Faraday Discuss.* **199**, 239 (2017).
- [12] Z. A. H. Goodwin and A. A. Kornyshev, *Electrochem. Comm.* **82**, 129 (2017).
- [13] R. Kjellander, *J. Chem. Phys.* **148**, 193701 (2018).
- [14] B. Rotenberg, O. Bernard, and J.-P. Hansen, *J. Phys. Condens. Matter* **30**, 054005 (2018).
- [15] F. Coupette, A. A. Lee, and A. Härtel, *Phys. Rev. Lett.* **121**, 075501 (2018).
- [16] R. M. Adar, S. A. Safran, H. Diamant, and D. Andelman, *Phys. Rev. E* **100**, 042615 (2019).
- [17] S. W. Coles, C. Park, R. Nikam, M. Kanduč, J. Dzubiella, and B. Rotenberg, *J. Phys. Chem. B* **124**, 1778 (2020).
- [18] J. Zeman, S. Kondrat, and C. Holm, *Chem. Commun.* **56**, 15635 (2020).
- [19] N. Anousheh, F. J. Solis, and V. Jadhao, *AIP Adv.* **10**, 125312 (2020).
- [20] R. Kjellander, *Phys. Chem. Chem. Phys.* **22**, 23952 (2020).
- [21] J. Zeman, S. Kondrat, and C. Holm, *J. Chem. Phys.* **155**, 204501 (2021).
- [22] A. Ciach and O. Patsahan, *J. Phys. Condens. Matter* **33**, 37LT01 (2021).
- [23] E. Krucker-Velasquez and J. W. Swan, *J. Chem. Phys.* **155**, 134903 (2021).
- [24] P. Cats, R. Evans, A. Härtel, and R. van Roij, *J. Chem. Phys.* **154**, 124504 (2021).
- [25] S. Kumar, P. Cats, M. B. Alotaibi, S. C. Ayirala, A. A. Yousef, R. van Roij, I. Siretanu, and F. Mugele, *J. Colloid Interface Sci.* **622**, 819 (2022).
- [26] S. Schön and R. von Klitzing, *Beilstein J. Nanotechnol.* **9**, 1095 (2018).
- [27] P. Simon and Y. Gogotsi, *Nat. Mater.* **7**, 845 (2008).
- [28] D. Brogioli, *Phys. Rev. Lett.* **103**, 058501 (2009).
- [29] A. Härtel, M. Janssen, D. Weingarth, V. Presser, and R. van Roij, *Energy Environ. Sci.* **8**, 2396 (2015).
- [30] S. Porada, R. Zhao, A. van der Wal, V. Presser, and P. Biesheuvel, *Prog. Mater. Sci.* **58**, 1388 (2013).
- [31] E. J. W. Verwey, J. T. G. Overbeek, and K. van Nes, *Theory of the Stability of Lyophobic Colloids: The Interaction of Sol*

- Particles Having an Electric Double Layer* (Elsevier Publishing Company, New York, 1948).
- [32] B. Derjaguin and L. Landau, *Prog. Surf. Sci.* **43**, 30 (1993).
- [33] Y. Li, M. Girard, M. Shen, J. A. Millan, and M. O. de la Cruz, *Proc. Natl. Acad. Sci. U.S.A.* **114**, 11838 (2017).
- [34] A. A. Kornyshev, D. J. Lee, S. Leikin, and A. Wynveen, *Rev. Mod. Phys.* **79**, 943 (2007).
- [35] J. R. Espinosa, M. Galván, A. S. Quiñones, J. L. Ayala, and S. M. Durón, *Sensors* **19**, 3956 (2019).
- [36] M. Shapiro, K. Homma, S. Villarreal, C.-P. Richter, and F. Bezanilla, *Nat. Commun.* **3**, 736 (2012).
- [37] A. C. L. de Lichtervelde, J. P. de Souza, and M. Z. Bazant, *Phys. Rev. E* **101**, 022406 (2020).
- [38] P. Debye and E. Hückel, *Phys. Z.* **24**, 185 (1923).
- [39] A. M. Smith, A. A. Lee, and S. Perkin, *Phys. Rev. Lett.* **118**, 096002 (2017).
- [40] P. Attard, C. P. Ursenbach, and G. N. Patey, *Phys. Rev. A* **45**, 7621 (1992).
- [41] R. Kjellander and D. J. Mitchell, *Chem. Phys. Lett.* **200**, 76 (1992).
- [42] R. Evans, J. R. Henderson, D. C. Hoyle, A. O. Parry, and Z. A. Sabeur, *Mol. Phys.* **80**, 755 (1993).
- [43] R. Evans, R. J. F. Leote de Carvalho, J. R. Henderson, and D. C. Hoyle, *J. Chem. Phys.* **100**, 591 (1994).
- [44] J. Ennis, R. Kjellander, and D. J. Mitchell, *J. Chem. Phys.* **102**, 975 (1995).
- [45] J. Ulander and R. Kjellander, *J. Chem. Phys.* **114**, 4893 (2001).
- [46] See Supplemental Material at <http://link.aps.org/supplemental/10.1103/PhysRevLett.130.108202> for details on the simulations, the fitting of decay lengths, and the derivation of the minimal cluster theory, which includes Refs. [47–60].
- [47] J.-P. Hansen and I. R. McDonald, *Theory of Simple Liquids*, 4th ed. (Elsevier, Oxford, 2013).
- [48] F. Weik, R. Weeber, K. Szuttor, K. Breitsprecher, J. de Graaf, M. Kuron, J. Landsgesell, H. Menke, D. Sean, and C. Holm, *Eur. Phys. J. Special Topics* **227**, 1789 (2019).
- [49] H. C. Andersen, J. D. Weeks, and D. Chandler, *Phys. Rev. A* **4**, 1597 (1971).
- [50] J. D. Weeks, D. Chandler, and H. C. Andersen, *J. Chem. Phys.* **54**, 5237 (1971).
- [51] R. W. Hockney and J. W. Eastwood, *Computer Simulation Using Particles* (IOP, London, 1988).
- [52] P. González-Mozuelos, G. I. Guerrero-García, and M. Olvera de la Cruz, *J. Chem. Phys.* **139**, 064709 (2013).
- [53] R. Evans, *Adv. Phys.* **28**, 143 (1979).
- [54] A. Härtel, *J. Phys. Condens. Matter* **29**, 423002 (2017).
- [55] R. Roth and D. Gillespie, *J. Phys. Condens. Matter* **28**, 244006 (2016).
- [56] Y. Rosenfeld, *Phys. Rev. Lett.* **63**, 980 (1989).
- [57] R. Roth, *J. Phys. Condens. Matter* **22**, 063102 (2010).
- [58] H. Hansen-Goos and R. Roth, *J. Phys. Condens. Matter* **18**, 8413 (2006).
- [59] J. K. Percus, *Phys. Rev. Lett.* **8**, 462 (1962).
- [60] H. L. Frisch and J. L. Lebowitz, *The Equilibrium Theory of Classical Fluids: A Lecture Note and Reprint Volume* (Benjamin, New York, 1964).
- [61] J. G. Kirkwood, *J. Chem. Phys.* **7**, 919 (1939).
- [62] R. J. F. Leote de Carvalho and R. Evans, *Mol. Phys.* **83**, 619 (1994).
- [63] G. Orkoulas and A. Z. Panagiotopoulos, *J. Chem. Phys.* **101**, 1452 (1994).
- [64] A.-P. Hynninen, M. E. Leunissen, A. van Blaaderen, and M. Dijkstra, *Phys. Rev. Lett.* **96**, 018303 (2006).
- [65] M. Bültmann and A. Härtel, *J. Phys. Condens. Matter* **34**, 235101 (2022).
- [66] J. Zwanikken and R. van Roij, *J. Phys. Condens. Matter* **21**, 424102 (2009).
- [67] F. W. Richey, B. Dyatkin, Y. Gogotsi, and Y. A. Elabd, *J. Am. Chem. Soc.* **135**, 12818 (2013).
- [68] M. A. Gebbie, M. Valtiner, X. Banquy, W. A. Henderson, and J. N. Israelachvili, *Proc. Natl. Acad. Sci. U.S.A.* **110**, E4122 (2013).
- [69] R. M. Adar, T. Markovich, and D. Andelman, *J. Chem. Phys.* **146**, 194904 (2017).
- [70] G. Feng, M. Chen, S. Bi, Z. A. H. Goodwin, E. B. Postnikov, N. Brilliantov, M. Urbakh, and A. A. Kornyshev, *Phys. Rev. X* **9**, 021024 (2019).
- [71] P. Jones, F. Coupette, A. Härtel, and A. A. Lee, *J. Chem. Phys.* **154**, 134902 (2021).
- [72] J. M. Dean, S. W. Coles, W. R. Saunders, A. R. McCluskey, M. J. Wolf, A. B. Walker, and B. J. Morgan, *Phys. Rev. Lett.* **127**, 135502 (2021).
- [73] Z. A. H. G. Goodwin, M. McEldrew, P. de Souza, M. Z. Bazant, and A. A. Kornyshev, *J. Chem. Phys.* **157**, 094106 (2022).
- [74] P. K. Jones, K. D. Fong, K. A. Persson, and A. A. Lee, *arXiv:2208.03182*.
- [75] T. Baimpos, B. R. Shrestha, S. Raman, and M. Valtiner, *Langmuir* **30**, 4322 (2014).